Distributed Hydrostatic Pressure Measurement Using Phase-OTDR in a Highly Birefringent Photonic Crystal Fiber

Sergei Mikhailov ⓘD, *Student Member, OSA*, Li Zhang ⓘD, Thomas Geernaert ⓘD, *Member, OSA*, Francis Berghmans ⓘD, *Senior Member, IEEE, Member, OSA*, and Luc Thévenaz ⓘD, *Fellow, IEEE, Fellow, OSA*

Abstract—Although distributed fiber-optic sensing of axial strain and temperature is a well-established technique, there are almost no demonstrations of distributed hydrostatic pressure sensing. The main obstacle for such measurements is the low sensitivity to pressure of standard optical fibers. Structured fibers, such as photonic crystal fibers, can be made pressure sensitive by means of an optimized arrangement of their internal microstructure. In this paper, we demonstrate—for the first time to our knowledge—distributed birefringence and hydrostatic pressure measurements based on phase-sensitive optical time-domain reflectometry (OTDR) in highly birefringent photonic crystal fibers. We study the response to hydrostatic pressure of two dedicated pressure-sensitive photonic crystal fibers in the range from ∼0.8 to ∼67 bar with a 5-cm spatial resolution using a phase-OTDR approach. We find differential pressure sensitivities between the slow and fast polarization axes of the studied fibers of –219 MHz/bar and 95.4 MHz/bar. These values are ∼3.8 to ∼8.8 times larger than those demonstrated previously in distributed pressure measurements with other photonic crystal fibers.

Index Terms—Birefringence, microstructured optical fibers, optical fiber sensors, pressure sensors, Rayleigh scattering, reflectometry.

I. INTRODUCTION

DISTRIBUTED optical fiber sensing (DOFS) of axial strain and temperature [1], [2] is a well-established technology, which has found its place in the market, and which is also still the subject of extensive research and innovation efforts. However, there are almost no demonstrations of DOFS of hydrostatic pressure [3]–[5]. The main obstacle to such measurements is the

small pressure sensitivity of standard step-index optical fibers [6]. Dedicated birefringent fibers may provide a solution to this shortcoming. An internal structure of airholes, such as that used to obtain the so-called 'side-hole fiber', can increase the pressure sensitivity [7]. A hydrostatic load applied to the coating or cladding of such a fiber can induce an asymmetric stress concentration in its core region, yielding a higher sensitivity of birefringence to pressure.

The birefringence of photonic crystal fibers (PCFs) can also be exploited for pressure sensing, with the advantage that PCFs can be designed to feature an enhanced pressure sensitivity by optimizing the layout of the holey microstructure in the fiber's cross-section [8]. In addition, PCFs are mostly manufactured of single pure silica material, unlike conventional birefringent fibers (Panda, Bow-tie), and their birefringence can also be tailored to be negligibly sensitive to temperature [9], [10]. Such PCFs could therefore offer a low to negligible pressure measurement cross-sensitivity to temperature. Despite the higher cost of PCFs when compared with conventional step-index fibers, they can still be economically relevant for the specialty application (pressure sensing) over relatively short sensing distances (up to several km) targeted here, since they form only a minor part of the total cost of the proposed distributed sensing system.

In this paper, we exploit this pressure sensing potential, and we demonstrate a distributed pressure measurement using a pressure-sensitive highly birefringent photonic crystal fiber and a phase-sensitive optical time-domain reflectometry (ϕOTDR) technique.

II. WORKING PRINCIPLE

Distributed pressure sensing in polarization maintaining fibers utilizing optical frequency domain reflectometry (OFDR) [3] and Brillouin dynamic gratings (BDGs) [4], [5] has already been demonstrated. However, OFDR is fundamentally limited in sensing fiber length [11] and BDG requires a rather complicated experimental setup [12]. OFDR indeed provides for a very high spatial resolution (down to sub-mm) at the expense of a relatively short sensing distance, which is limited by the coherence length of the light source. The BDG approach is in principle not limited in sensing distance and allows for measurements with sub-meter spatial resolution, but requires three high-power lightwaves with different precisely controlled
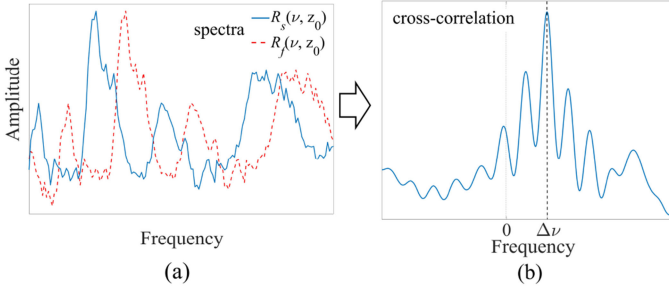
Fig. 1. Illustration of the principle of operation of a distributed birefringence measurement based on ϕOTDR. (a) Local Rayleigh spectra at a position z_0 along both orthogonally polarized modes of the birefringent fiber. The frequency shift between these two local spectra leads to (b) a crosscorrelation peak at $\Delta\nu$.

Fig. 2. (a) Frequency shifts $\Delta\nu(P)$ obtained via cross-correlations of ϕOTDR signals of a reference measurement and measurements at different applied pressures converted into (b) pressure-induced changes of refractive indices $\Delta n(P)$ along the slow and fast polarization axes as function of pressure.

frequencies and polarizations for generating and interrogating the dynamic grating. The use of BDGs also requires access to both fiber ends, which can limit the application potential.

Our approach exploits the detection of pressure-induced phase modal birefringence changes ΔB by means of ϕOTDR [13]. This technique exploits Rayleigh backscattering along the fiber, caused by random density fluctuations in the fiber core, that have arisen during the manufacturing of the fiber, and those scattering centers are "frozen" in the fiber. Phase-OTDR method provides for a performance that is similar to that of BDGs, but with a simpler interrogation scheme.

In ϕOTDR, highly coherent laser pulses launched into the fiber under test are backscattered by refractive index variations along the fiber. By scanning the frequency of the light source, one can obtain local reflection spectra at each sensing point of the fiber. These spectra have an irregular shape and they are static under constant environmental conditions, but changes in environmental parameters such as temperature and strain lead to changes of the refractive index and thereby of the optical path length. This can be compensated by an appropriate frequency shift $\Delta\nu$ of the interrogating light pulse at a frequency ν [12]. That frequency shift $\Delta\nu$ then provides an indication for the local refractive index change.

A. Phase Birefringence Measurement

In order to find the distribution of the phase birefringence B along the fiber, we measure the Rayleigh spectra $R_s(\nu, z_0)$ and $R_f(\nu, z_0)$ for both orthogonally polarized slow and fast optical axes of the fiber, at each position z_0. Because of the difference in refractive index of these two modes, the local spectra are shifted in frequency with respect to each other. Therefore, their cross-correlation function $C(\Delta\nu, z_0) = R_s(\nu, z_0) * R_f(\nu, z_0)$ (Fig. 1) features a maximum at the frequency $\Delta\nu = \nu_s - \nu_f$, corresponding to the phase birefringence $B = n_s - n_f$ as given by [13]:

$$\Delta\nu = \frac{\nu_f}{n_f^g}B, \qquad (1)$$

where ν_s, ν_f, n_s, n_f are frequencies and refractive indices along the two orthogonal slow and fast polarization axes, and n_f^g is the group refractive index along the fast axis.
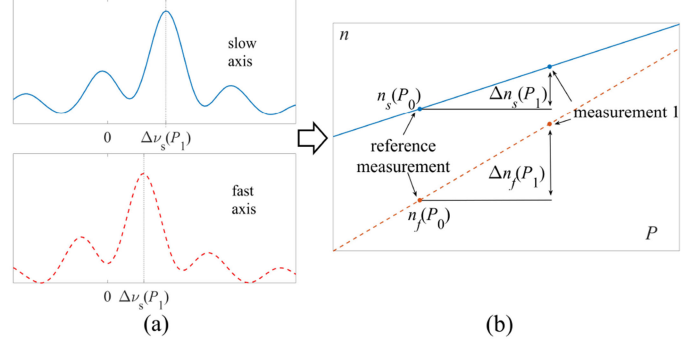
B. Pressure Measurement

Although it is possible to obtain information about the applied pressure by comparing the absolute value of the birefringence in an optical fiber, calculated according to (1), to a reference value for B, we encountered technical difficulties with polarization alignment of a scanning pulse along the optical axes of the fiber, limiting the accuracy of the measured birefringence. Also, random birefringence fluctuations along the fiber length lead to amplitude reduction and spectral broadening of the cross-correlation peak. In addition, large frequency shifts (larger than the width of the correlation peak), corresponding to high birefringence values, give rise to large errors in the birefringence and, consequently, in applied pressure estimation [14]. We therefore use a slightly modified approach for pressure measurements. We retrieve the pressure-induced birefringence change along the fiber by calculating the spectral cross-correlations of ϕOTDR traces from a reference measurement at a known pressure P_0 and measurements at applied pressure P_i, $i = 1, 2, \ldots$ for each of the orthogonal polarization axes. Owing to the nature of Rayleigh backscattered signal, the same reference is valid for multiple pressure measurements if the measurement setup parameters do not change in time. The cross-correlation function $C_{s,f}(\Delta\nu, z_0, \Delta P_i) = R_{s,f}(\nu, z_0, P_0) * R_{s,f}(\nu, z_0, P_i)$ is now maximal at the frequency $\Delta\nu$, proportional to the equivalent pressure-induced changes of the refractive indices Δn_s and Δn_f along the slow and fast polarization axes (Fig. 2):

$$\Delta\nu_{s,f} = \frac{\nu_{s,f}}{n_{s,f}^g}\Delta n_{s,f} \qquad (2)$$

After obtaining the Δn values for the fast and slow axes, we calculate the change of the phase birefringence as follows:

$$\Delta B_i = \Delta n_s(P_i) - \Delta n_f(P_i), i = 1, 2 \ldots \qquad (3)$$

This way the fluctuations of the refractive index along each polarization axis—giving rise to random variations of the birefringence—do not directly impact on the contrast of the correlation, since these fluctuations are steadily present in each measurement. The differential refractive index changes with pressure along each axis is therefore representative of and scaled by the average birefringence over the spatial resolution.
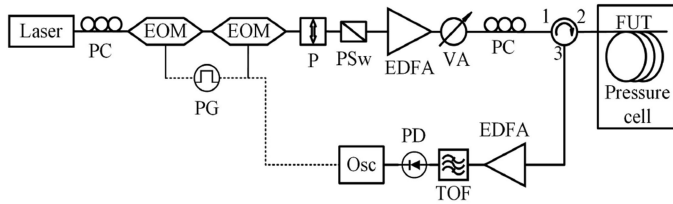
Fig. 3.   Scheme of the experimental ϕOTDR setup used for the distributed pressure measurement. Abbreviations are explained in the text.

(a)   (b)

Fig. 4.   Scanning electron microscope images of the cross-sections of the two microstructured fibers under test. (a) Fiber A. (b) Fiber B.

The main drawback of this measurement is that it only provides the pressure-induced change of the birefringence ΔB, but not its absolute value B. The relation between ΔB and $\Delta P = P_{i+1} - P_i$ is fiber dependent and is usually given by a simple linear relation [15], [16]. Hydrostatic pressure that is applied to the fiber cladding (or coating) creates an asymmetric stress distribution in the core region owing to the asymmetric cross-section of the fiber. Via the stress-optic effect this translates into the introduction of material birefringence in the core region and thereby in a measurable change of the phase modal birefringence.

III. EXPERIMENTAL SETUP

Figure 3 shows the scheme of the experimental ϕOTDR setup. We used a distributed feedback (DFB) laser emitting at a wavelength around 1551 nm with a linewidth of 3 MHz. We placed a polarization controller (PC) before the electro-optical modulators (EOMs) to optimize the optical power. To form a scanning pulse with a duration of 500 ps (yielding a 5 cm spatial resolution) with high extinction ratio ($\sim$60 dB), we used two cascaded EOMs driven by pulse generators, and we tuned the current of the laser driver to scan the pulse frequency. A polarizer (P) and polarization switch (PSw), placed after the EOMs, defined the orthogonal states of polarization of the interrogating pulse. An erbium-doped fiber amplifier (EDFA) amplified the optical pulses, whilst a variable attenuator (VA) controlled the pulse power entering the fiber under test (FUT). We also used a second PC for aligning the pulse polarization along one of the polarization axes of the FUT. An optical circulator was used to launch the interrogation pulse into the FUT and collect the backscattered signal. The backscattered light was collected from port 3 of the circulator and amplified by an EDFA. We also used a tunable optical filter to reduce the amplified spontaneous emission added by the EDFA. Finally, we detected the backscattered signal with a 3-GHz bandwidth photodetector (PD) and recorded it with a 10-GSps oscilloscope (Osc). All spectra were recorded with 1000 averages to reduce the measurement noise.

IV. EXPERIMENTAL RESULTS

A. Phase Birefringence Measurement

We carried out our measurements using 2 highly birefringent (HiBi) "Butterfly" PCFs [17], further denoted as fibers A and B, with cross-sections shown in Fig. 4. These PCFs feature high polarimetric pressure sensitivities $K_P = 2\pi/\lambda dB/dP$, while
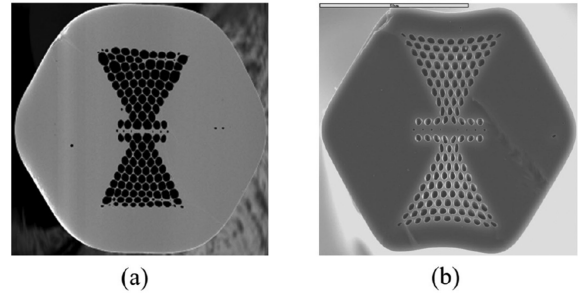
their polarimetric temperature sensitivities $K_T = 2\pi/\lambda dB/dT$ and polarimetric strain sensitivities $K\varepsilon = 2\pi/\lambda dB/d\varepsilon$ are almost zero. Owing to their low cross-sensitivity of the birefringence to pressure and temperature, these Butterfly fibers are candidates of choice for experimenting with distributed pressure sensing. Earlier measurements [18] have shown that the average phase modal birefringence B of the 26.5 m-long fiber A is $7.2 \cdot 10^{-4}$ (corresponding to $\Delta \nu \approx 99.6$ GHz), and the birefringence of the 48 m-long fiber B is $1.7 \cdot 10^{-4}$ at $\lambda = 1550$ nm ($\Delta \nu \approx 22.8$ GHz). The propagation losses in the studied PCFs are $\sim$24 dB/km.

Upfront knowledge of the approximate birefringence level allowed us to decrease the broad frequency scanning of more than 100 GHz for determination of the birefringence distribution. We tuned the frequency of the interrogating pulses, aligned to the slow and fast axes, to a difference $\Delta \nu$ with respect to each other and we scanned it in a range of 28.9 GHz with 64.5 MHz steps. We calculated the cross-correlations of the ϕOTDR traces obtained from two consecutive measurements for orthogonal polarization axes along each fiber, with 5 cm spatial resolution, as shown in Fig. 5. One complete set of measurements took approximately 6 minutes. Based on the known frequency shifts, we obtained the corresponding birefringence distributions using equation (1). Fig. 5 shows that the birefringence distributions (blue lines) in the studied PCFs are considerably nonuniform over their length (standard deviation of B is $1.5 \cdot 10^{-5}$ for fiber A and $2.75 \cdot 10^{-5}$ for fiber B, several times larger than in commercially available PCFs [5], [19]), which is mainly attributed to small variations in the airhole microstructure along the fiber. The nonuniformity of the birefringence distribution can also be partially caused by additional strain variations induced by spooling. Nevertheless, the mean value of the measured birefringence of fiber A $7.64 \cdot 10^{-4}$ agrees well with the result given above. The average birefringence in fiber B ($2.5 \cdot 10^{-4}$) is larger than specified, but given the pronounced nonuniformity this may be due to the selection of the portion over which measurements have been made.

B. Pressure Measurement

We studied the dependence of the birefringence variations on applied pressure. To do so we placed the fiber section of about 5.5 m long in an oil pressure chamber. We increased the pressure from atmospheric to about 68 bar. Temperature variations throughout the total duration of the experiment
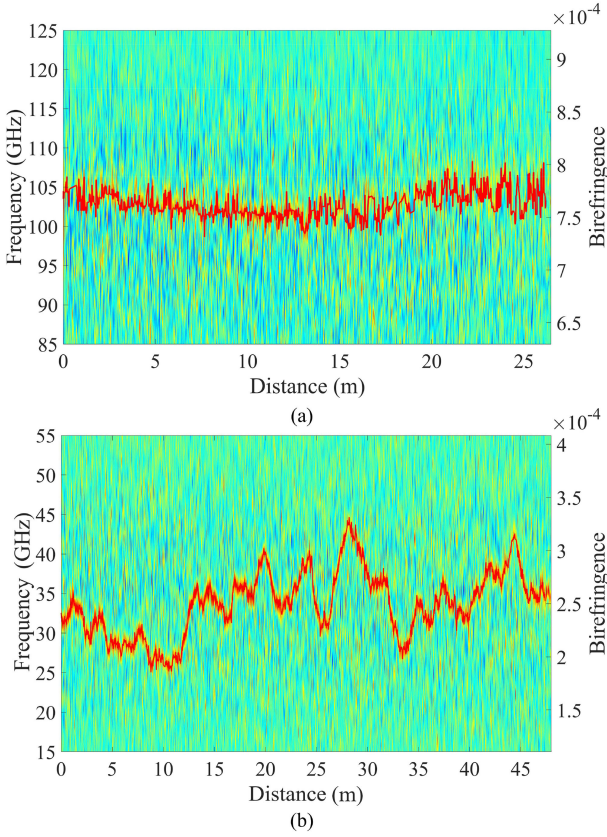
Fig. 5. Phase birefringence distribution along (a) fiber A and (b) fiber B. The left vertical axis gives the measured frequency shift, whilst the right vertical axis gives the calculated phase birefringence.
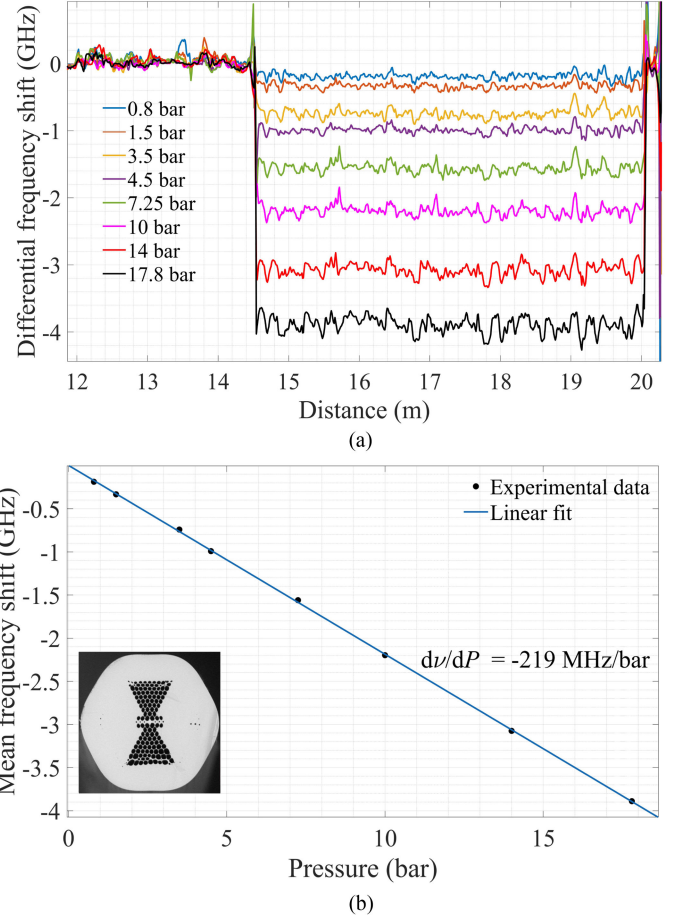

Fig. 6. (a) DiffFS distributions along the fiber A under various applied pressures, (b) mean frequency shift in the fiber A as a function of pressure change.

(∼3-4 hours) were less than 2 °C and, considering the very low temperature sensitivity ($d\nu/dT \sim 2$ MHz/K), these temperature variations could be neglected. We took reference measurements at atmospheric pressure.

The distributions of the pressure induced differential frequency shifts (DiffFS) for fibers A and B are shown in Fig. 6(a) and Fig. 7(a), respectively. The birefringence decreases with increasing pressure and the pressure responses of the fibers are slightly non-uniform. Such behavior can be caused by variations of the airhole microstructure along the fiber, small fluctuations of the polarization state of the scanning pulse over measurement time and pressure leakage from the chamber during the measurements (up to ∼0.2 bar/min).

Fig. 6(b) and Fig. 7(b) show the mean values of the differential frequency shift in the pressurized PCFs as a function of the applied pressure. We calculate the pressure sensitivities $d\nu/dP$ from linear fits of the experimental data and we find -219 MHz/bar for fiber A (corresponding polarimetric pressure sensitivity $K_P = -66$ rad·MPa^{-1}·m^{-1}) and -95.4 MHz/bar for fiber B (corresponding polarimetric pressure sensitivity $K_P = -28.6$ rad · MPa^{-1}·m^{-1}). These values are in a good agreement with the results of previous measurements (-59 rad·MPa^{-1}·m^{-1} and -29 rad·MPa^{-1}·m^{-1} for fibers A and B, respectively) [16], [17], and are ∼8.8 and ∼3.8 times higher than K_P of PCFs previously reported (-7.5 rad·MPa^{-1}· m^{-1})

[3], [5]. We used the variations of the DiffFS along unpressurized portions of the fibers to calculate the standard deviations of the measurements. We found ∼49 MHz (corresponding to a pressure uncertainty of 0.22 bar) for fiber A, and ∼52 MHz (pressure uncertainty of 0.59 bar) for fiber B.

V. SUMMARY AND CONCLUSION

We presented, for the first time to our knowledge, distributed pressure measurements using ϕOTDR in two dedicated pressure sensitive PCFs. We obtained a pressure sensitivity that is ∼3.8 to ∼8.8 times larger than that reported in other proposed distributed pressure measurements with PCFs. We have shown that our technique allows for sub-bar measurement resolution (up to 0.3 bar for the fiber with the highest pressure sensitivity and a frequency scanning resolution of 64.5 MHz). The maximal sensing length is limited by the high propagation losses of the studied fibers (∼24 dB/km) and is of the order of a few hundred meters with our experimental setup if the spatial resolution of 5 cm is preserved. A longer sensing distance would require fibers with lower propagation losses, otherwise an increased width of the interrogating pulses is required. Longer pulses lead to lower spatial resolutions, but at the same time they reduce the spectral
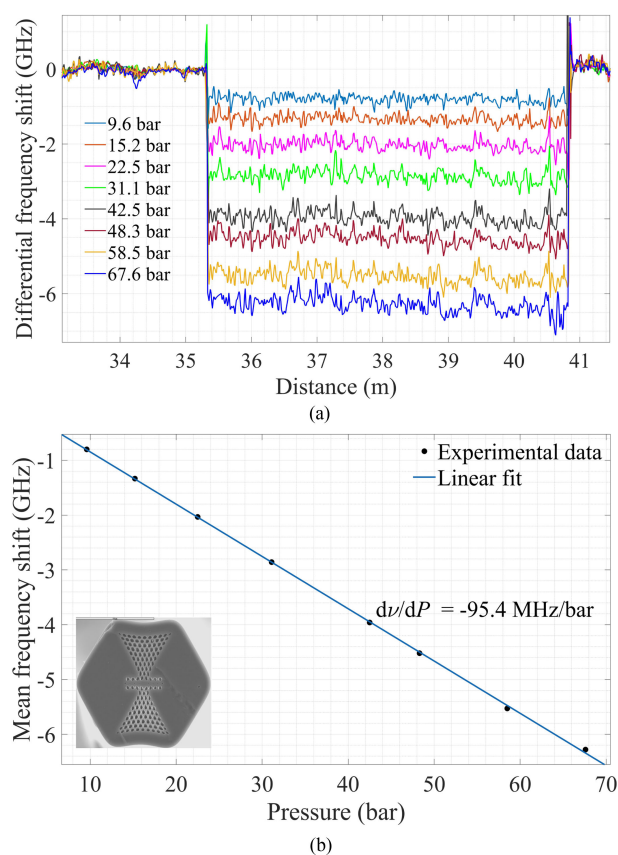
Fig. 7. (a) DiffFS distributions along the fiber B under various applied pressures, (b) mean frequency shift in the fiber B as a function of pressure change.

width of the correlation peak, allowing for a more precise estimation of the birefringence change. Therefore, there is a trade-off between the spatial resolution and the birefringence resolution. The pressure resolution can be further improved by implementing a finer pulse frequency tuning and a better control over the polarization state of the interrogating pulse. The main limitation of the measurements, based on the detection of changes in the birefringence, stems from the fast fluctuations (shorter than the spatial resolution) of the birefringence along the fiber, leading to broadening and amplitude reduction of the correlation peak. Resolving smaller pressure variations therefore calls for improving the uniformity of the birefringence along the fiber.

REFERENCES

[1] T. Horiguchi, K. Shimizu, T. Kurashima, M. Tateda, and Y. Koyamada, "Development of a distributed sensing technique using Brillouin scattering," *J. Lightw. Technol.*, vol. 13, no. 7, pp. 1296–1302, Jul. 1995, doi: 10.1109/50.400684.

[2] Y. Koyamada, M. Imahama, K. Kubota, and K. Hogari, "Fiber-optic distributed strain and temperature sensing with very high measurand resolution over long range using coherent OTDR," *J. Lightw. Technol.*, vol. 27, no. 9, pp. 1142–1146, May 2009, doi: 10.1109/JLT.2008.928957.

[3] T. Chen *et al.*, "Distributed high-temperature pressure sensing using air-hole microstructural fibers," *Opt. Lett.*, vol. 37, no. 6, pp. 1064–1066, 2012, doi: 10.1364/OL.37.001064.

[4] Y. H. Kim, H. Kwon, J. Kim, and K. Y. Song, "Distributed measurement of hydrostatic pressure based on Brillouin dynamic grating in polarization maintaining fibers," *Opt. Express*, vol. 24, no. 19, pp. 21399–21406, 2016, doi: 10.1364/OE.24.021399.

[5] L. Teng *et al.*, "Temperature-compensated distributed hydrostatic pressure +sensor with a thin-diameter polarization-maintaining photonic crystal fiber based on Brillouin dynamic gratings," *Opt. Lett.*, vol. 41, no. 18, pp. 4413–4416, 2016, doi: 10.1364/OL.41.004413.

[6] S. Le Floch, and P. Cambon, "Study of Brillouin gain spectrum in standard single-mode optical fiber at low temperatures (1.4–370 K) and high hydrostatic pressures (1–250 bars)," *Opt. Commun.*, vol. 219, no. 1/6, pp. 395–410, 2003, doi: 10.1016/S0030-4018(03)01296-3.

[7] H. M. Xie, P. Dabkiewicz, R. Ulrich, and K. Okamoto, "Side-hole fiber for fiber-optic pressure sensing," *Opt. Lett.*, vol. 11, no. 5, pp. 333–335, 1986, doi: 10.1364/OL.11.000333.

[8] M. Szpulak, T. Martynkien, and W. Urbanczyk, "Effects of hydrostatic pressure on phase and group modal birefringence in microstructured holey fibers," *Appl. Opt.*, vol. 43, no. 24, pp. 4739–4744, 2004, doi: 10.1364/AO.43.004739.

[9] T. Nasilowski *et al.*, "Temperature and pressure sensitivities of the highly birefringent photonic crystal fiber with core asymmetry," *Appl. Phys. B*, vol. 81, no. 2/3, pp. 325–331, 2005, doi: 10.1007/s00340-005-1900-8.

[10] X. Dong, H. Y. Tam and P. Shum, "Temperature-insensitive strain sensor with polarization-maintaining photonic crystal fiber based Sagnac interferometer," *Appl. Phys. Lett.*, vol. 90, no. 15, 2007, Art. no. 151113, doi: 10.1063/1.2722058.

[11] M. Froggatt and J. Moore, "High-spatial-resolution distributed strain measurement in optical fiber with Rayleigh scatter," *Appl. Opt.*, vol. 37, no. 10, pp. 1735–1740, 1998, doi: 10.1364/AO.37.001735.

[12] K. Y. Song, W. Zou, Z. He and K. Hotate, "Optical time-domain measurement of Brillouin dynamic grating spectrum in a polarization-maintaining fiber," *Opt. Lett.*, vol. 34, no. 9, pp. 1381–1383, 2009, doi: 10.1364/OL.34.001381.

[13] M. A. Soto, X. Lu, H. F. Martins, M. Gonzalez-Herraez, and L. Thévenaz, "Distributed phase birefringence measurements based on polarization correlation in phase-sensitive optical time-domain reflectometers," *Opt. Express*, vol. 23, no. 19, pp. 24923–24936, 2015, doi: 10.1364/OE.23.024923.

[14] L. Zhang, Z. Yang, F. Gyger, M. A. Soto and L. Thévenaz, "Rayleigh-based distributed optical fiber sensing using least mean square similarity," presented at the 26th Int. Conf. Optical Fiber Sensors, Lausanne, Switzerland, Sep. 24–28, 2018.

[15] J. R. Clowes, S. Syngellakis, and M. N. Zervas, "Pressure sensitivity of side-hole optical fiber sensors," *IEEE Photon. Technol. Lett.*, vol. 10, no. 6, pp. 857–859, Jun. 1998, doi: 10.1109/68.681509.

[16] Z. Zhu and T. G. Brown, "Stress-induced birefringence in microstructured optical fibers," *Opt. Lett*, vol. 28, no. 23, pp. 2306–2308, 2003, doi: 10.1364/OL.28.002306.

[17] T. Martynkien *et al.*, "Highly birefringent microstructured fibers with enhanced sensitivity to hydrostatic pressure," *Opt. Express*, vol. 18, no. 14, pp. 15113–15121, 2010, doi: 10.1364/OE.18.015113.

[18] S. Sulejmani *et al.*, "Control over the pressure sensitivity of Bragg grating-based sensors in highly birefringent microstructured optical fibers," *IEEE Photon. Technol. Lett.*, vol. 24, no. 6, pp. 527–529, Mar. 2012, doi: 10.1109/LPT.2012.2183120.

[19] H. Zhang, Z. Yuan, Z. Liu, W. Gao and Y. Dong, "Simultaneous measurement of strain and temperature using a polarization-maintaining photonic crystal fiber with stimulated Brillouin scattering," *Appl. Phys. Express*, vol. 10, 2016, Art. no. 012501, doi: 10.7567/APEX.10.012501.